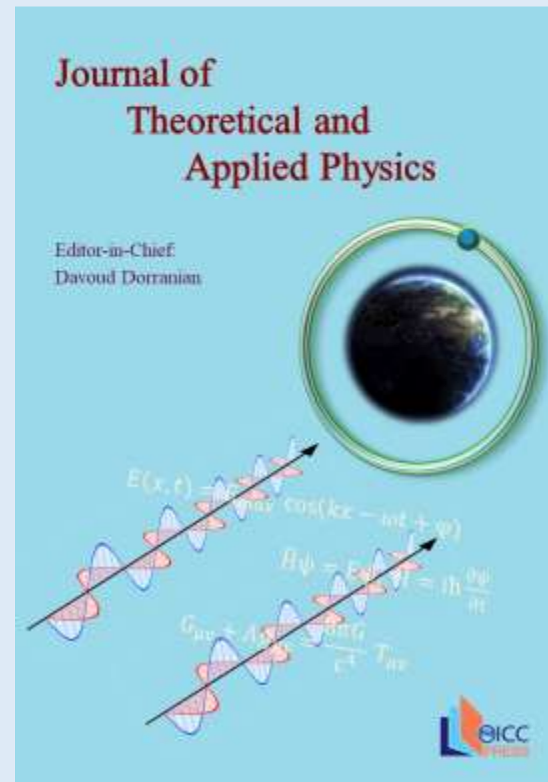

Optical imaging and magnetic field simulation of a DC circular planar magnetron sputtering discharge

Ahmad Reza Rastkar[1], Ali Reza Niknam[1], Mostafa Salahshoor[2]

[1]*Laser and Plasma Research Institute, Shahid Beheshti University, Tehran, Iran*

[2] *School of Physics, Iran University of Science and Technology, Tehran, Iran*

Corresponding author: a-rastkar@sbu.ac.ir

Received: 20 February 2023;

Accepted: 09 May 2023;

http://dx.doi.org/10.57647/J.JTAP.2023.1704.38

Optical imaging and magnetic field simulation of a DC circular planar magnetron sputtering discharge

Ahmad Reza Rastkar[1], Ali Reza Niknam[1], Mostafa Salahshoor[2]

[1]Laser and Plasma Research Institute, Shahid Beheshti University, Tehran

[2] School of Physics, Iran University of Science and Technology, Tehran, Iran

a-rastkar@sbu.ac.ir

Abstract. In this paper, the optical images of glow discharge plasma and the finite element method simulation of the magnetic field strength in a balanced and two types of unbalanced DC circular planar magnetron sputtering sources are presented. The investigation showed that wherever the magnetic field strength is stronger, the intensity of light and the ionization are greater and consequently, the deposition is higher. The comparison of recorded optical images with the finite element simulation results of the magnetic field strength indicated the correlation between regions of high magnetic field strength and high light emission.

Keywords: glow discharge plasma, magnetron sputtering, magnetic field distribution, Finite Element Method.

ACCEPTED PAPER

1 Introduction

Direct-current (DC) magnetron sputtering devices have been widely used for many years to deposit metallic thin films on various substrates [1-10]. The sputtering technique among other deposition methods has many advantages such as lower substrate temperature, more precise control of the deposition rate, integration for large area applications and etc [11-13]. Many experimental and simulation investigations have been conducted on magnetron sputtering discharges [14-18]. Window and Savvides have considered seven circular planar magnetron sputtering sources of essentially the same geometry but using different magnet designs and studied the charged particle fluxes from these sources [19]. They have shown that on each side of a balanced magnetic arrangement there are two classes of unbalanced magnetic designs which they have called type I and type II. The authors have also indicated that the magnetic field configuration can be varied to change the operation between these two types of design and to adjust the flux of electrons or ions. Sheridan et al [20] have measured the electron velocity distribution function in the azimuthal direction in a sputtering magnetron discharge by using a one-sided, planar Langmuir probe. Kondo and Nanbu have presented a self-consistent numerical analysis of a planar DC magnetron discharge by use of the particle-in-cell/Monte Carlo (PIC/MC) method and clarified its structure with an axisymmetric magnetic field [21]. Shidoji et al [22] have numerically studied the characteristics of the plasma structure in both an unbalanced magnetron and balanced magnetron under differing arrangements of the magnetic field distribution. The plasma discharge characteristics of a DC magnetron device have been measured by Wu [23] using a single Langmuir probe at the center axis of the dual-side process chamber. Seo et al [24] have experimentally investigated the electron drift and the loss balance of charged particles in the downstream region of an unbalanced DC magnetron Argon discharge. Seo et al [25] have also studied the plasma dynamics in DC and short-pulse magnetron discharges using spatially and temporally resolved single Langmuir probe measurements. Kolev and Bogaerts have proposed a self-consistent approach, based on the PIC/MC collision method, to study the process of sputtering and the behavior of the sputtered atoms in a DC magnetron. They have also demonstrated the generation, transport, and deposition of the sputtered atoms from a copper cathode [26]. Kageyama et al [27] have simulated the plasma confinement in DC magnetron sputtering under different magnetic arrays and electrode (anode) structures by using the two-dimensional hybrid model. The role of Ohmic heating of electrons in a DC magnetron discharge has been demonstrated by Brenning et al [28]. Aghilizadeh et al [29] studied the role of oxygen content added to the argon as a working gas on a thin copper oxide layer deposited by DC magnetron sputtering. In this way, they showed that the optical behavior, phase composition, and structure of the copper thin films can be controlled. Ryabinkin et al [30] have performed a two-dimensional PIC/MC simulation to study the plasma of an axially symmetric planar DC magnetron discharge in argon. Recently, Abid et al [31] reported a review on the synthesis of nanomaterials and they discussed the use of the plasma magnetron sputtering technique to grow and synthesize amorphous nanostructured thin film.

ACCEPTED PAPER

The aforementioned works have shown that the magnetic field plays an important role in magnetron sputtering operation. In these works, however, there is not an investigation about the influence of the magnetic field distribution on the light emission profile. The magnetic field forces the electrons to rotate in circular orbits. This leads to enhance the confinement of the electrons, and consequently to increase the likelihood of ionization and excitation collisions. Therefore, variations in the spatial profile of the magnetic fields would have considerable impacts on the plasma properties and in turn the light emission profile.

In the present work, we have provided a comparison between the light

emission profile and the magnetic field distribution in a homemade DC circular planar magnetron sputtering device. We have presented the optical images of plasma glow discharge for three different cases. We have also simulated the distributions of the magnetic field, the electric field, and the electric potential of the device employing the finite element (FE) code, ANSYS [32]. Moreover, we have demonstrated the dependency of the light intensity profiles on the magnetic field distributions. Finally, we have discussed the transparency or opacity of the deposited layers.

This work is organized into four sections. In Section II, we present the basic considerations for the experimental study of DC circular planar magnetron sputtering sources and the FE simulation of the magnetic field strength in these sources. In Section III, the simulation and experimental results for three different magnetrons are discussed. Finally, a summary and conclusion are given in Section IV.

2 Experimental and Simulation Consideration

ACCEPTED PAPER

Figures 1(a) and 1(b) show schematic diagrams of the magnetron sputtering system and the hypothetical magnetic field lines under the magnetron. In our homemade magnetron device, the central magnet is a solid cylindrical permanent magnet with the diameter of 15 mm and the outer magnet is a hollow cylindrical permanent magnet with inner and outer diameter of 50 mm and 70 mm, respectively. The distance from the target to the substrate in the sputtering chamber is 50 mm. The height of the magnets is 15 mm. A ferromagnetic soft iron plate was employed to prevent the leakage of magnetic flux to the undesired region and to achieve proper magnetic field distribution between target and substrate. The diameter and thickness of the soft iron plate are 70 mm and 5mm respectively. The discharge experiments were carried out at -500 V and 4 Pa as the cathode voltage and working pressure, respectively, and the anode of the magnetron was grounded [6].

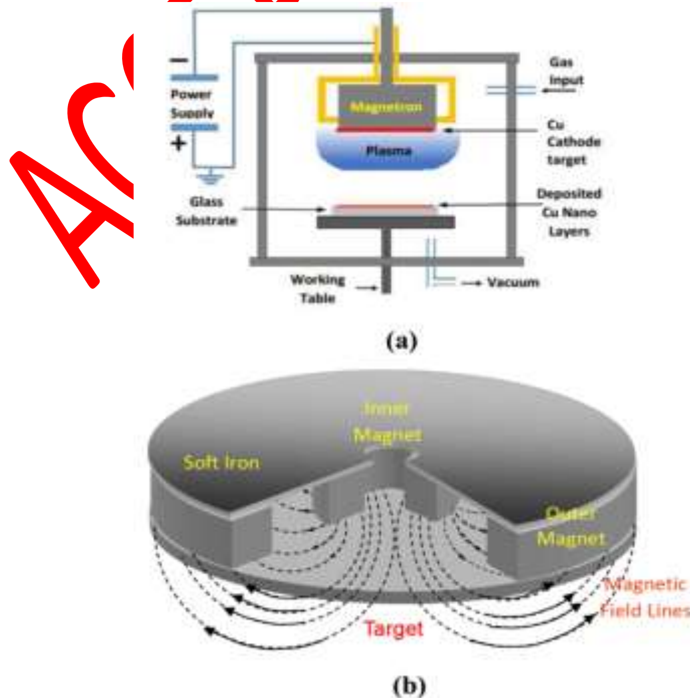

Figure 1. (a) Schematic representation of the magnetron sputtering system and (b) Schematic diagram of magnetic field lines as typically found in a magnetron source.

The configuration of the simulation model is based on our homemade magnetron sputtering device. Because of the cylindrical symmetry of the magnetron structure, a 2D axisymmetric model was used, instead of the real 3D model. We have simulated the static (time-independent) electric and magnetic fields of the magnetron sputtering cathode using the ANSYS code. It uses finite element analysis to solve the Maxwell equations. In our study, we have solved the Laplace and Ampere equations for calculating the electric and magnetic fields, respectively. For the magnetostatic problem, the magnetic scalar potential is assumed to be zero at the exterior boundaries of the model. We have also used the zero-potential boundary condition for the electrostatic problem. Relative permeability and coercive force of permanent magnets were chosen as the properties of the magnetic materials for simulation. The relative permeability of soft iron plate was chosen equal to 1500 for all models. The target was oxygen free high conductivity copper with a purity of 99.99% as a non-magnetic material [6]. Magnetic properties of different ferrite permanent magnets for balanced and two types of unbalanced magnetrons (UNB1 and UNB2), are listed in Table 1.

Table 1. Magnetic properties of different ferrite permanent magnets for balanced and two types of unbalanced magnetron.

	Balanced		Unbalanced (UNB1)		Unbalanced (UNB2)	
Property	Central Magnet	Outer Magnet	Central Magnet	Outer Magnet	Central Magnet	Outer Magnet
Relative Permeability (x 1000)	1.5	1.5	1.5	1.5	1.5	1.5
Coersive Force (kA/m)	150	150	900	150	30	150

ACCEPTED PAPER

3 Results and Discussion

Variation in the strength and distribution of the magnetic field in a magnetron sputtering configuration affect the plasma parameters; the light intensity, the energy flux, the deposition rate and consequently the opacity of the coating. Therefore, in this study, we have considered the magnetic field distributions for different magnetic field configurations. Figure 2 shows the simulated magnetic flux density (B field) in Gauss unit and emission profile images of a balanced and two types of unbalanced magnetron around a 70 mm target. The results of the simulations are obtained in the steady state and the optical images are taken when the discharge is stable. In figure 2, we use a logarithmic scale for presenting the magnetic field distribution more clearly. We have also shown the magnetic flux lines for a better understanding of the trajectories of the electrons. Our results are qualitatively consistent with the results of Window and Savvides. In the balanced magnetron, the optical image (Fig. 2(a)) and calculated flux density (Fig. 2(b)) are distributed which are in contrast to those of unbalanced magnetrons (Fig. 2(c) and Fig. 2(d) or Fig. 2(e) and Fig. 2(f)). In the first case of unbalanced magnetron, the magnetic flux density is more concentrated around the central magnet by increasing the magnetic strength of this magnet (Fig. 2(d)). The magnetic flux density is however more dispersed towards the outer magnet for the UNB2 configuration (Fig. 2(f)) by decreasing the magnetic strength of the central magnet. Figure 2 shows that the FE simulation results of the magnetic field strength correlate with the optical images of the light-intensity distributions. This correlation can be interpreted as follows: In a magnetron source, the ionization degree

of the generated glow discharge is increased by the presence of the magnetic field strength and consequently the trapped electrons. Also, the light emission originates from the de-excitation of metastable energy states of the gas atoms and ions. Given that the emission intensity of light from the electron-impact excited species in the plasma is proportional to the electron density and the density of the excited species [33], therefore the intensity of light is greater where the strength of the magnetic field is stronger.

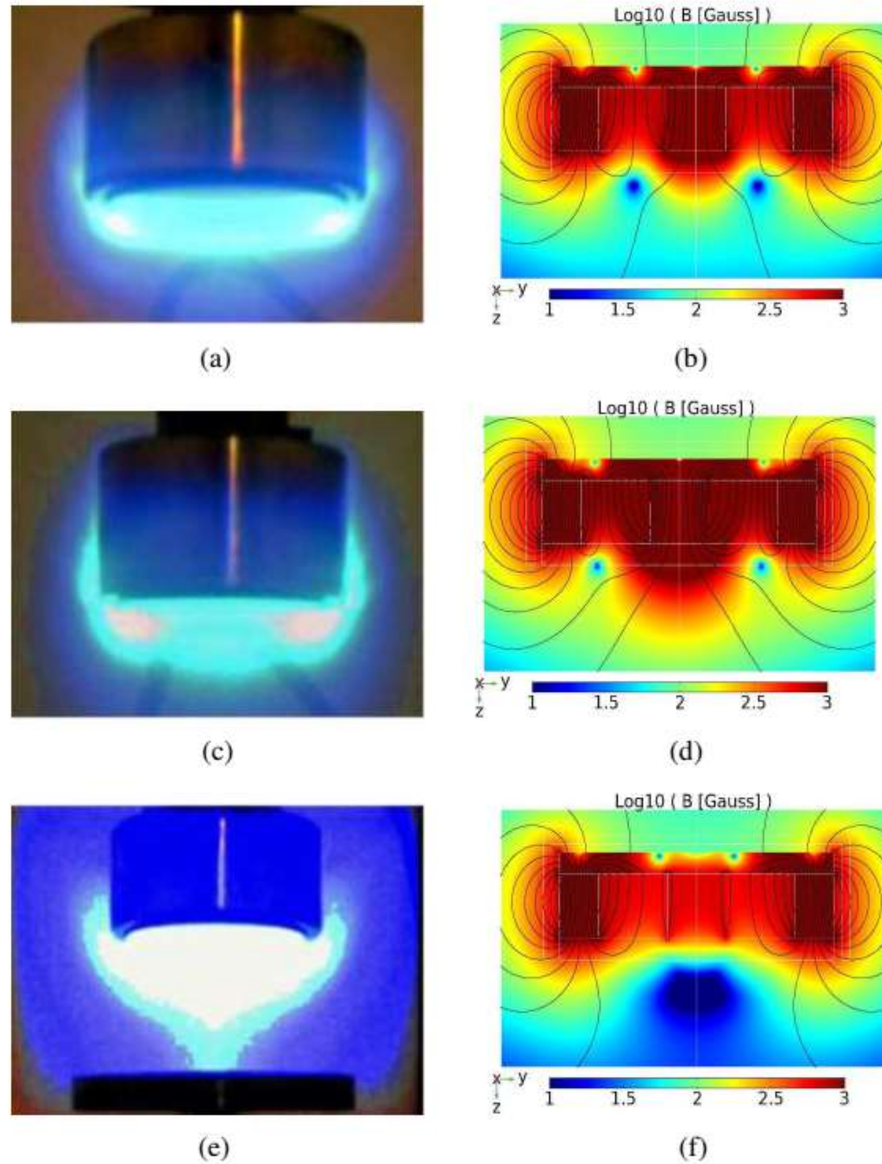

Figure 2. Optical images of light emission and simulated magnetic flux density (in Gauss) in a magnetron sputtering source with the cathode voltage of -500 V and the working pressure 4 Pa are shown for balanced magnetron (a) and (b), first type unbalanced magnetron (c) and (d) and second type unbalanced magnetron (e) and (f). These definitions are qualitatively according to Window and Savvides.

We also present the plots of the electric field and potential distributions in Figs. 3(a) and 3(b), respectively, to follow the cross angle between the B-field and the E-field. These figures are nearly the same for all three types of magnetrons because the permanent magnets have little effect on the electric field and potential distributions.

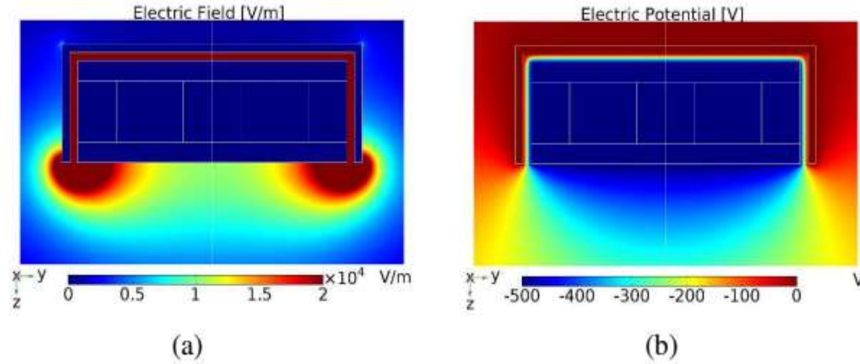

Figure 3. Plots of the simulated electric field (a) and potential (b) distributions.

Figures 4(a), 4(b) and 4(c) show the photo-response of coated copper films on glass substrates corresponding to the three different magnetrons corresponding to Figs. 2(a), 2(c) and 2(e) respectively. From these figures, it could be suggested that in the balanced magnetron with a coercive force of 150 kA/m, the distribution of the coating is not smooth and the outermost ring of the coating is thicker than the inner rings (Fig. 4(a)). This could be due to the greater strength of the outer magnet that has a higher impact on the deposition rate. With increasing the coercive force of the inner magnet (UNB1 with 900 KA/m), this distribution varies and a relatively smooth coating is made overall the substrate (Fig. 4(b)). In other words, the coating tends to be more uniform across the diameter of the round substrate. In the case of the less coercive force of the inner magnet (UNB2 with 30 KA/m), the effect of inner magnet could be neglected and the coating will be affected only by the outer magnet (Fig. 4(c)). As well-known, the ion bombardment of a film during the growth process can improve the film properties. Based on the magnetic field distribution of the UNB2 magnetron configuration we can use from this configuration to induce ion bombardment on the substrate. Therefore, the UNB2 magnetron configuration, where the outer pole is stronger than the central pole, is a more appropriate configuration because in this case, the magnetic field distribution is such that one can obtain a higher ion current density at the substrate during the deposition process.

Figures 5(a), 5(b), and 5(c) illustrate the atomic force microscopy (AFM) topography images related to Figs. 4(a), 4(b), and 4(c), respectively, and Fig. 5(d) indicates the AFM image of the glass substrate as a comparison.

ACCEPTED

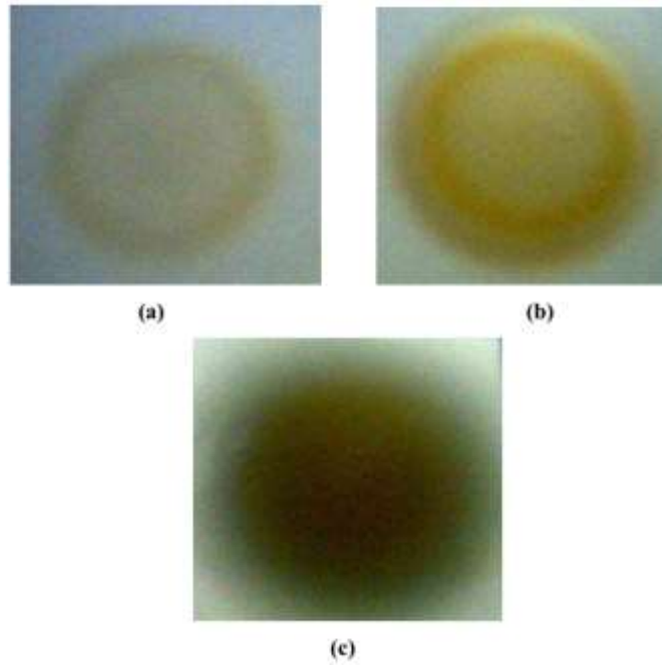

Figure 4. Images (a), (b) and (c) are the samples coated with copper on a glass substrate with the three different types of magnetron magnet packs shown in Figs. 2(a), 2(c) and 2 (e) respectively. The transparency and color of the copper on the glass varied from (a) to (c).

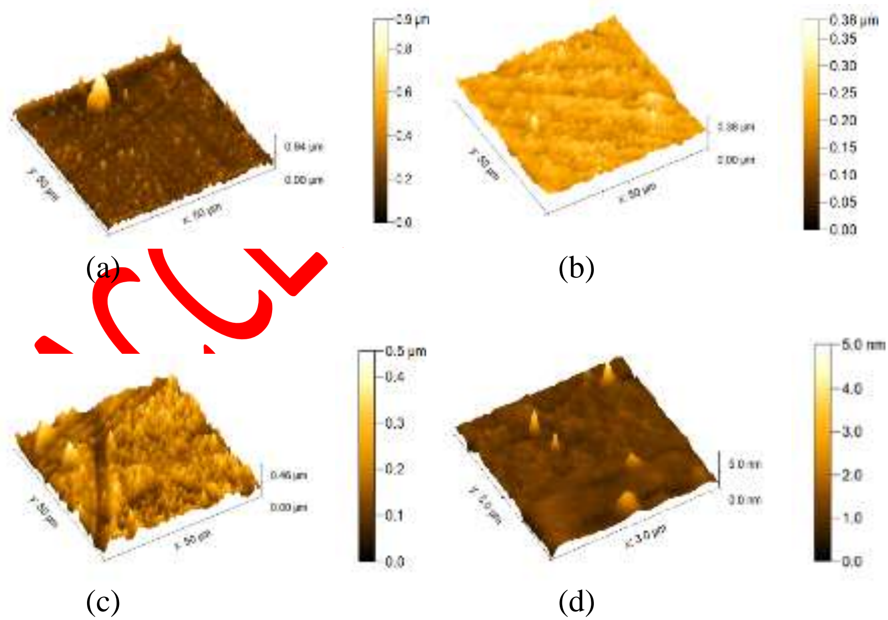

Figure 5. AFM images (a), (b), and (c) are related to the samples presented in Figs. 4(a), 4(b) and 4(c), respectively, and (d) is related to the glass substrate as a comparison.

4 Conclusions

In this study, we presented optical images of a DC glow discharge plasma for the balanced and two types of unbalanced circular planar magnetron configurations. We compared these images with the corresponding simulated magnetic field distributions. The FE simulation of the magnetic field distribution in the magnetron sputtering source showed that this distribution is non-uniform. Therefore, the optical emission of the discharge is non-uniform [34]. The comparison of the recorded images to the simulation results indicated the correlation between regions of high magnetic field strength and high light emission. In these regions, the ionization degree and the ion density are higher which results in an enhanced sputtering and a change in the deposition profile. The comparison between the balanced and two types of unbalanced magnetron sources in terms of magnetic field strengths showed that by an appropriate choice of the magnetic field configurations, one can provide a controllable ion flux and consequently can enhance the efficiency of the deposition processes. The results indicated that the UNB2 configuration with a strong outside magnet can give a larger ion flux at substrates [19].

ACCEPTED PAPER

References

[1] J. R. Roth, Industrial plasa engineering, Volume 1: Principles, Institute of Physics Publishing, Bristol and Philadelphia, 1995.

[2] J. R. Roth, Industrial plasma engineering, Volume 2: Applications to nonthermal plasma processing, CRC press, 2001.

[3] M. A. Lieberman and A. J. Lichtenberg, Principles of plasma discharges and materials processing, John Wiley & Sons, 2005.

[4] J. G. Han, *Journal of Physics D: Applied Physics,* **42**:043001, 2009.

[5] A. R. Rastkar, A. R. Niknam, and B. Shokri, *Thin Solid Films*, **517**:5464, 2009.

[6] M. Siemers, A. Pflug, T. Melzig, K. Gehrke, A. Weimar, and B. Szyszka, *Surface and Coatings Technology*, **241**:50, 2014.

[7] S. Gauter, F. Haase, and H. Kersten, *Thin Solid Films*, **669**:8, 2018.

[8] A. Poladi, H. M. Semnani, E. Emadoddin, F. Mahboubi, and H. Ghomi, *Ceramics International*, **45**:8095, 2019.

[9] A. Heidarnia and H. Ghom, *Journal of Theoretical and Applied Physics (JTAP)*, **16**:162217, 2022.

[10] A. Granmayeh Rad and H. Abbasi, *Journal of Theoretical and Applied Physics (JTAP)*, **17**:172304, 2023.

[11] K. Ellmer, *Journal of Physics D: Applied Physics*, **33**:R17, 2000.

[12] G. Bräuer, B. Szyszka, M. Vergöhl, and R. Bandorf, *Vacuum*, **84**:1354, 2010.

[13] N. Abid, A. M. Khan, S. Shujait, K. Chaudhary, M. Ikram, M. Imran, J. Haider, M. Khan, Q. Khan, and M. Maqbool, *Advances in Colloid and Interface Science*, **300**:102597, 2022.

[14] E. Shidoji, N. Nakano, and T. Makabe, *Thin Solid Films*, **351**:37, 1999.

[15] Y. Xiang, W. Chengbiao, L. Yang, Y. Deyang, and X. Tingyan, *Plasma Science and Technology*, **8**:337, 2006.

[16] E. Bultinck and A. Bogaerts, *Journal of Physics D: Applied Physics*, **41**:202007, 2008.

[17] M. Zhang, X. Zhou, X. Wang, and C. Deng, *Ceramics International*, **47:**31357, 2021.

[18] J. D. Castro, M. J. Lima, and S. Carvalho, *Applied Surface Science*, **584**:152582, 2022.

[19] B. Window and N. Savvides, *Journal of Vacuum Science & Technology A*, **4**:196, 1986.

[20] T. Sheridan, M. Goeckner, and J. Goree, *Journal of Vacuum Science & Technology A: Vacuum, Surfaces, and Films*, **16**:2173, 1998.

[21] S. Kondo and K. Nanbu, *Journal of Physics D: Applied Physics*, **32**:1142, 1999.

[22] E. Shidoji, E. Ando, and T. Makabe, *Plasma Sources Science and Technology*, **10**:621, 2001.

[23] S. Wu, *Journal of Applied Physics*, **98**:083301, 2005.

[24] S.-H. Seo, J.-H. In, and H.-Y. Chang, *Journal of Applied Physics*, **97**:023305, 2005.

[25] S.-H. Seo, J.-H. In, and H.-Y. Chang, *Plasma Sources Science and Technology*, **15**:256, 2006.

[26] I. Kolev and A. Bogaerts, *Journal of Vacuum Science & Technology A: Vacuum, Surfaces, and Films*, **27**:20, 2009.

[27] J. Kageyama, M. Yoshimoto, A. Matsuda, Y. Akao, and E. Shidoji, *Japanese Journal of Applied Physics*, **53**:088001, 2014.

[28] N. Brenning, J. T. Gudmundsson, D. Lundin, T. Minea, M. A. Raadu, and U. Helmersson, *Plasma Sources Science and Technology*, **25**:065024, 2016.

[29] N. Aghilizadeh, A. H. Sari, and D. Dorranian, *Journal of Theoretical and Applied Physics (JTAP)*, **11**:285, 2017.

[30] A. N. Ryabinkin, A. O. Serov, A. F. Pal, Yu. A. Mankelevich, A. T. Rakhimov, and T. V. Rakhimova, *Plasma Sources Science and Technology*, **30**:055009, 2021.

[31] N. Abid, A. M. Khan, S. Shujait, K. Chaudhary, M. Ikram, M. Imran, J. Haider, M. Khan, Q. Khan, M. Maqbool, *Advances in Colloid and Interface Science*, **300**:102597, 2022.

[32] Ansys Mechanical APDL Low-Frequency Electromagnetic Analysis Guide, ANSYS, Release 12.0. ANSYS, Inc. 2009.

[33] S. M. Rossnagel and K. L. Saenger, *Journal of Vacuum Science & Technology A*, **7**:968, 1989.

[34] F. Debal, F. Cammarata, M. Wautelet, J. P. Dauchot, and M. Hecq, *Journal of Physics D: Applied Physics*, **31**:L31, 1998.

ACCEPTED PAPER